Investigating the Synergistic Effects of Cascaded ST-LHTES Unit and CEG with PCM on Thermal Performance: A Numerical Study

Narender Kumar[1], Chandrashekhar Bhardwaj[1] and Prodyut R. Chakraborty[1*]

[1] Indian Institute of Technology Jodhpur, Rajasthan (India)

[*] Corresponding Author

Abstract

Latent heat based thermal energy storage systems (LHTES) have gained interest for their high energy storage density and isothermal energy charging and discharging. However, challenges such as low thermal conductivity and performance enhancement must be addressed. The promising solution for this is using a cascading of PCMs combined with compressed expanded graphite (CEG). In this study, cascading is considered by employing two phase change materials (PCMs), Lithium Nitrate (PCM 1) and Solar Salt (PCM 2), arranged axially along the heat transfer fluid (HTF) flow direction (Therminol-66). Numerical simulations using ANSYS Fluent 2019 R2 is conducted to investigate the charging dynamics of a 2-D axisymmetric shell and tube LHTES unit. A volume fraction-updating scheme is used to study the melt fraction of PCMs in all cases. Moreover, the proposed model will analyze the exergy efficiency and effectiveness of LHTES.

Keywords: Latent Heat, Compressed Expanded Graphite, Cascading, Charging and Discharging

1. Introduction

With the global pursuit of sustainable alternatives to fossil fuels, the prominence of solar energy is rapidly surging as an increasingly favored option. However, efficient solar energy exploitation requires thermal energy storage (TES) to store surplus energy and supply it during shortages. Among the TES categories, latent heat thermal energy storage (LHTES) is the most suitable due to its high energy storing capacity under nearly isothermal conditions [Khan et al., 2016]. LHTES uses phase change materials (PCMs) that store or release latent heat energy during melting or solidification. However, one of the major constraint that limits its usage corresponds to its lower thermal conductivity which narrows down the rate of heat transfer and hinders their further significance [Wu et al., 2017]. In corresponds to refine the thermal capability, numerous techniques have been implemented to improve thermal conductivity, incorporating metal fins [Kumar and Verma, 2020], diffusing high conductivity nanoparticles [Colla et al., 2017], appending heat pipes [Zhao et al. 2016], PCM embedded in metal foam [Zheng et al., 2018] and compressed expanded graphite (CEG) [Mallow et al., 2016; Mills et al., 2006] to form a composite. Nevertheless, among the aforementioned approaches, incorporating phase change material (PCM) into composite encapsulated graphite (CEG) appears to be the most efficient strategy for enhancing thermal conductivity. This is primarily due to several benefits it offers, such as superior conductivity, enhanced thermal contact, cost-effectiveness, and ease of molding.

One other way to improve thermal performance is to cascade the thermal energy storage (CTES) systems, incorporating multiple phase change materials (PCMs), by ensuring a consistent temperature difference between the PCMs and the heat transfer fluid (HTF) in the direction of flow. To accomplish this, arrange PCMs during the charging process in decreasing order of their melting temperatures. CTES has shown superior storage performance compared to conventional LHTES systems that use a single PCM. Few studies have explored the benefits of cascaded PCM-based thermal energy storage (TES). Farid and Kanzawa (1989) and Farid et al. (1990) introduced the advantages of cascaded PCM TES and demonstrated significant overall performance improvements. Gong and Mujumdar (1996, 1997) study the effect of different PCM melting temperature arrangements with different thermo-physical properties and boundary conditions on charging and discharging processes. The results revealed that the charging-discharging rate improved by 35% for the multiple PCM units compared with the single PCM unit. Wang et al. (1999) proposed arranging multiple PCMs in a parabolic profile to reduce phase change time. Li et al. (2012) studied the exergy analysis of two phase change materials for solar thermal power and found that the melting temperatures of PCM1 and PCM2 have different influences on the overall exergy efficiency. Considering a wide gap in the literature, a numerical model is proposed that investigates the combined effect of cascading and CEG on LHTES.

10.18086/swc.2023.03.05 Available at http://proceedings.ises.org

2. Problem Statement

In the present work, the cycle dynamics of the 2-D axisymmetric shell and tube LHTES unit is investigated numerically. A dual approach is employed to enhance the performance of the storage unit. This involves cascading the LHTES unit and augmenting the effective thermal conductivity of the PCM through the incorporation of CEG while maintaining a constant volume constraint. A cascade of two PCMs is arranged axially along the flow direction of heat transfer fluid (HTF) to ensure the optimal utilization of the storage material. PCMs selected for energy storage are lithium nitrate (melting point: 253 °C) and solar salt which is a binary eutectic mixture of $NaNO_3$ and KNO_3 in the ratio of 60:40 by weight) (melting point: 238 °C). For heat transfer from source to PCM, Therminol-66 is selected as HTF. The arrangement of PCM is such that their melting temperature decreases along the HTF flow direction during charging. Cascading precisely addresses this concern by incorporating a second PCM (lower melting temperature), thereby maintaining the driving potential for heat transfer. An increase in the effective thermal conductivity of the PCM leads to a reduction in total melting time as well as performance enhancement of the LHTES unit. ANSYS Fluent 2019 R2 is used for the simulations, where the volume fraction-updating scheme will estimate the melt fraction of both PCMs. The energy conservation equation is considered diffusion-dominated in the PCM domain (due to the presence of the CEG matrix), while the k-ϵ model is adopted for turbulent flow in the HTF zone. The default energy equation and solidification/melting models available in Fluent solver is switched off; instead, a user defined scalar (UDS) is developed in C++ language for energy equation along with various UDFs for volume fraction updating scheme, anisotropic conductivity in PCM, velocity profile and source terms, and are hooked to ANSYS Fluent 2019 R2 solver.

Four Cases are considered for the study:

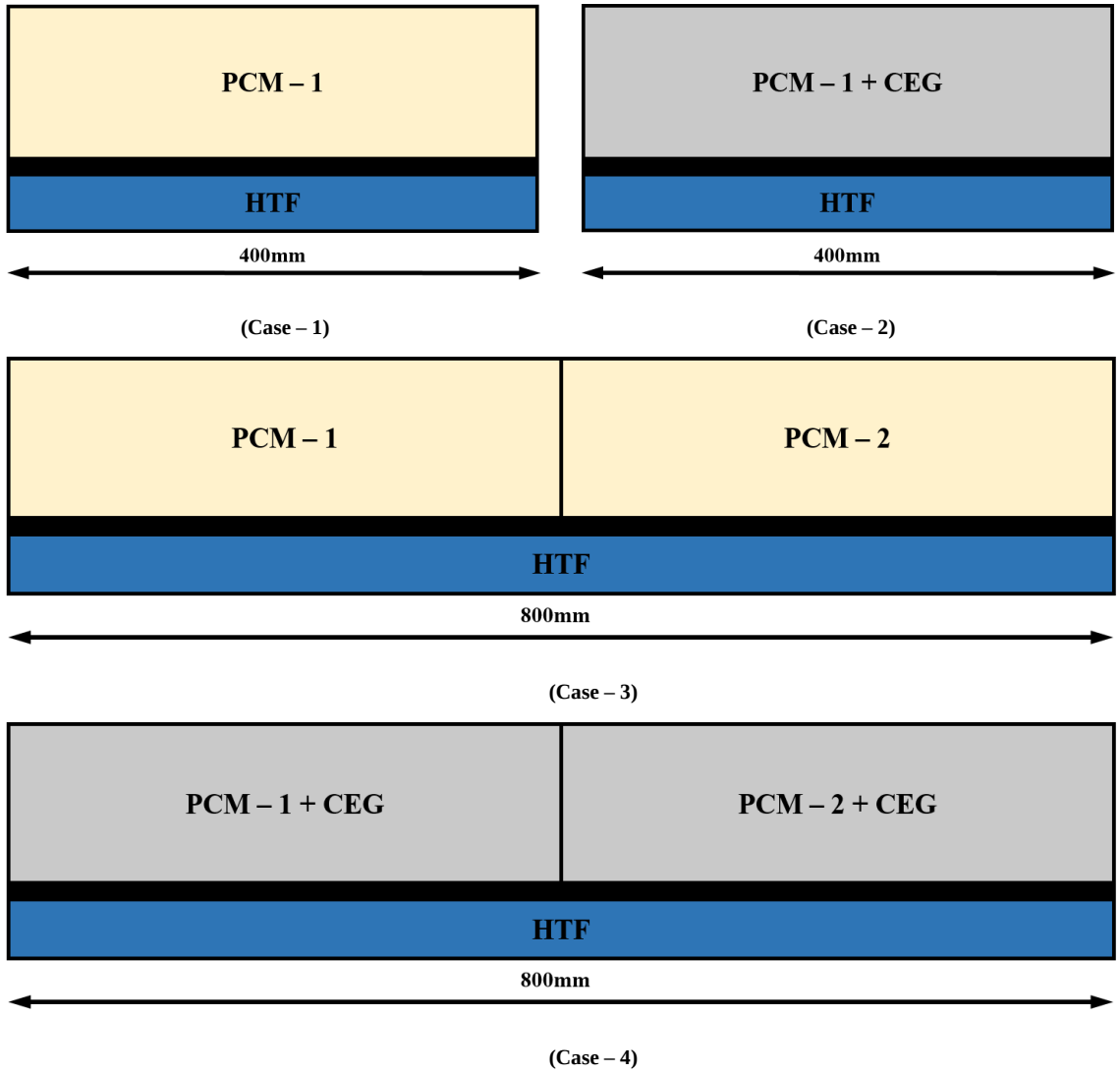

Fig. 1: Axisymmetric shell and tube LHTES unit for all four cases

As seen in Fig. 1, case - 1 and 2 are single PCM storage without CEG and with CEG respectively, and case – 3 and 4 are double cascaded storage unit without and with CEG respectively.

The analysis will be helpful to design LHTES unit for thermal energy storage applications considering volume constraints where multiple enhancement techniques are included simultaneously. The size of the domain is crucial for analysis, being viewed as a specific component within the ST-type latent heat storage unit. This unit comprises 100 tubes, all of the same size, and the shell side is also assumed to be identical to that of the storage unit.

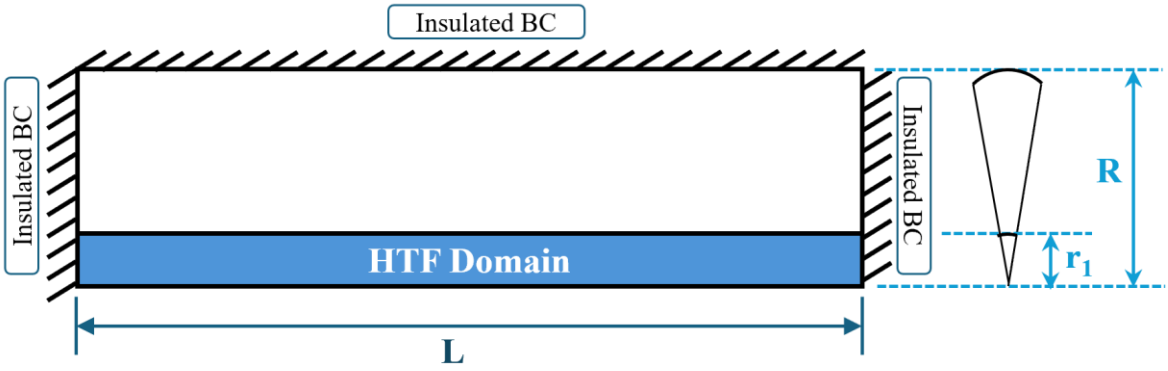

Fig. 2: Boundary conditions of the domain

L = 400 mm, R = 16.86 mm, r_1 = 4.62 mm

Tab. 1: Initial Conditions and Boundary Conditions

	PCM	HTF
Initial Conditions	T(x,r,0) = 237 °C, $[r_1 \leq r \leq R]$	T(x,r,0) = 237 °C , $[0 \leq r \leq r_1]$
Boundary Conditions	$(\frac{dT}{dx})_{(0,r,t)} = 0$, $[r_1 \leq r \leq R]$ $(\frac{dT}{dx})_{(L,r,t)} = 0$, $[r_1 \leq r \leq R]$ $(\frac{dT}{dr})_{(x,R,t)} = 0$, $[0 \leq x \leq L]$	T(0,r,t) = T_in °C, $[0 \leq r \leq r_1]$

Tab. 2: Properties of PCMs

The properties of $LiNO_3$ are sourced from Mohamed et al. (2016), while the properties of Solar Salt are referenced from Iverson et al. (2012) and EG from Xia et al. (2010). All properties are at temperature 30 °C.

PCM	Melting Temperature (°C)	Heat of Fusion(kJ/kg)	Thermal conductivity (W/m-K)	Density (kg/m^3)	Specific heat (J/kg-K)	
					Solid	Liquid
$LiNO_3$	253	373	0.51	2380	1688.5465	2015.1447
Solar Salt	238	109.8	0.5	1938.625	1850	1550
EG	-	-	25	270	690	719

Tab. 3: Properties of Therminol-66 (HTF)

Operating Temperature(°C)	Density (kg/m^3)	Specific Heat(J/kg-K)	Thermal conductivity (W/m-K)	Dynamicviscosity (N-s/m^2)
300	809	2570	0.0946	0.000413

3. Modelling

3.1. Assumptions

- Assuming PCM domain as 2-D axisymmetric.
- Diffusion heat transfer is dominated within the PCM domain.
- The effect of shrinkage in PCM is neglected.
- Axial heat conduction in HTF is neglected and is justified by high L/D ratio of the pipe.

- HTF does not change its phase.
- Materials properties are kept constant.
- Buoyancy (gravity) is not considered.

3.2. Mathematical Modelling

A mathematical model has been developed to investigate the heat transmission and charging characteristics in a horizontal shell and tube LHTES system for single unit and cascading system. The numerical modelling of phase change processes presents challenges due to the intricate interplay of thermal energy transfer between the PCM and HTF domain. Moreover, it is essential to address the nonlinear effects resulting from the absorption or release of substantial latent heat, along with addressing the transient properties arising from the motion of the solid-liquid interface. In the context of multiphase transport phenomena, Bennon and Incropera (1987) introduced a comprehensive conservation equation utilizing a fixed-grid volume averaging technique. The energy conservation equation within the CPCM is expressed as follows:

$$(1-g_g)(\rho_{PCM}c_{ps})\frac{\partial T}{\partial t} = \nabla.(k\nabla T) - (\rho_{PCM}h_{sl})\frac{\partial g_l}{\partial t} - \rho_{PCM}(c_{pl}-c_{ps})\frac{\partial}{\partial t}[g_l(T-T_m)] - (\rho_g c_{pg} g_g)\frac{\partial T}{\partial t} \quad \text{(eq. 1)}$$

Where, g, h, k, ρ, and T represents volume fraction, specific enthalpy, thermal conductivity, mass density and temperature respectively. Subscripts g, pcm, s and l stand for graphite, PCM, solid phase and liquid phase present in PCM-Graphite composite. Since shrinkage during slid-liquid phase transition is neglected, $\rho_l = \rho_s = \rho_{PCM} \neq \rho_g$, and the volume averaged density of PCM-Graphite composite is represented as $\rho = g_l\rho_l + g_s\rho_s + g_l\rho_l + g_g\rho_g$. For solid and liquid phases of PCM, and graphite, the specific enthalpies are defined as: $h_s = c_{ps}T$, $h_l = c_{ps}T_m + h_{sl} + c_{pl}(T-T_m)$ and $h_g = c_{pg}T$ respectively. The volume fraction of PCM in the PCM-graphite composite is identical to pore volume fraction in CEF foam and given by $\varepsilon = 1 - g_g = g_l + g_s$. Here we define a field parameter φ_l, defined as $\varphi_l = g_l/\varepsilon$. Here, we define a field parameter φ_l essentially represents the melt fraction () within the pore and varies within the range $0 \leq \varphi_l \geq 1$.

Now, for the HTF in the circular pipe; the 1- D energy conservation equation proposed by Morisson, et al. (2008) is as follows:

$$\rho_f \frac{\partial}{\partial t}(c_{pf}T_f) + \dot{G}\frac{\partial}{\partial x}(c_{pf}T_f) = \frac{2}{r}h(T_{wall} - T_f) \quad \text{(eq. 2)}$$

Where, h is convective heat transfer coefficient between HTF and wall of the pipe (A constant value of 1000 W/(m^{2}K) is assumed, with further elaboration provided by Morisson et al. (2008)), the subscript f is for the heat transfer fluid (HTF), $\dot{G}$ is the mass flux (kg/m^2 s) and r denotes the radius of pipe.

3.3. Energy Analysis

The rate of actual heat transfer $\dot{Q_{act}}$ (W) from HTF to heat storage unit for single and cascaded unit respectively was calculated by the following equation:

In case of single storage unit:

$$\dot{Q_{act}} = \dot{m}_f c_{pf}(T_{in} - T_{out}) \quad \text{(eq. 3)}$$

In case of double storage (cascaded TES) unit:

$$\dot{Q_{act}} = \dot{m}_f c_{pf}\{(T_{in1} - T_{out1}) - (T_{in2} - T_{out2})\} \quad \text{(eq. 4)}$$

As the outlet temperature of the first storage is the inlet of the second, (i.e. $T_{out1} = T_{in1}$)

$$\dot{Q_{act}} = \dot{m}_f c_{pf}(T_{in1} - T_{out2}) \quad \text{(eq. 5)}$$

The rate of maximum heat transfer $\dot{Q_{max}}$ (W) from HTF to heat storage unit was calculated by the following equation:

In case of single storage unit:

$$\dot{Q_{max}} = \dot{m}_f c_{pf}(T_{in} - T_m) \quad \text{(eq. 6)}$$

In case of double storage (cascaded TES) unit:

$$\dot{Q_{max}} = \dot{m}_f c_{pf}\{(T_{in1} - T_{m1}) - (T_{in2} - T_{m2})\} \quad \text{(eq. 7)}$$

As the outlet temperature of the first storage is the inlet of the second, (i.e. $T_{in2} = T_{m1}$) therefore we can write:

$$\dot{Q_{max}} = \dot{m}_f c_{pf}(T_{in1} - T_{m2}) \quad \text{(eq. 8)}$$

The heat transfer analysis of TES is quite similar to that of a heat exchanger, where heat transfers between HTF and PCM. Therefore, the effectiveness of the charging processes in the LHTES can be found as the ratio of the actual heat transfer to the maximum

$$\varepsilon = \frac{\dot{Q}_{act}}{\dot{Q}_{max}} \quad \text{(eq. 9)}$$

For single PCM unit:

$$\varepsilon = \frac{\dot{m}_f c_{pf}(T_{in} - T_{out})}{\dot{m}_f c_{pf}(T_{in} - T_m)} \quad \text{(eq. 10)}$$

For double PCM unit:

$$\varepsilon = \frac{\dot{m}_f c_{pf}(T_{in1} - T_{out2})}{\dot{m}_f c_{pf}(T_{in1} - T_{m2})} \quad \text{(eq. 11)}$$

The actual heat transfer rate is calculated according to the difference in HTF inlet and outlet temperature in both (i.e. single as well as in double PCMs unit) cases. However, the calculation of maximum heat transfer rate assumes that; the HTF outlet temperature approaches towards the minimum temperature of the system (i.e., melting temperature of PCM). In the case of cascading, the minimum melting temperature PCM is placed at the end of the system, which also ensures that the HTF temperature would be minimum. Thus, the effectiveness of the system is calculated by eq. 10 and eq. 11 for the single and cascaded storage unit.

4. Results and Discussion

In the present numerical analysis, four different cases are considered and simulations are performed to obtain melting fraction, isothermal plot, HTF outlet temperature versus time plot, average temperature of PCMs and for the efficiency analysis.

Case 1: Pure Lithium Nitrate ($LiNO_3$) is used as PCM in LHTES.

Case 2: Composite PCM ($LiNO_3$ + 11.11% graphite) is used for thermal energy storage in LHTES.

Case 3: Cascaded system of energy storage; $LiNO_3$ as PCM-1 and Solar salt as PCM-2, are considered for the analysis.

Case 4: Cascaded system of energy storage; PCM-1 ($LiNO_3$ + 11.11% graphite) and PCM-2 (Solar salt + 11.11% graphite) are considered for the analysis.

All the cases were simulated for different HTF inlet conditions (T_{in} = 300, 280, 260 ℃).

4.1. Effect of Graphite

Comparison between case-1 & 2 and case-3 & 4 is done after 500 seconds of each case to show the effect of anisotropy in thermal conductivity of PCM composite on charging.

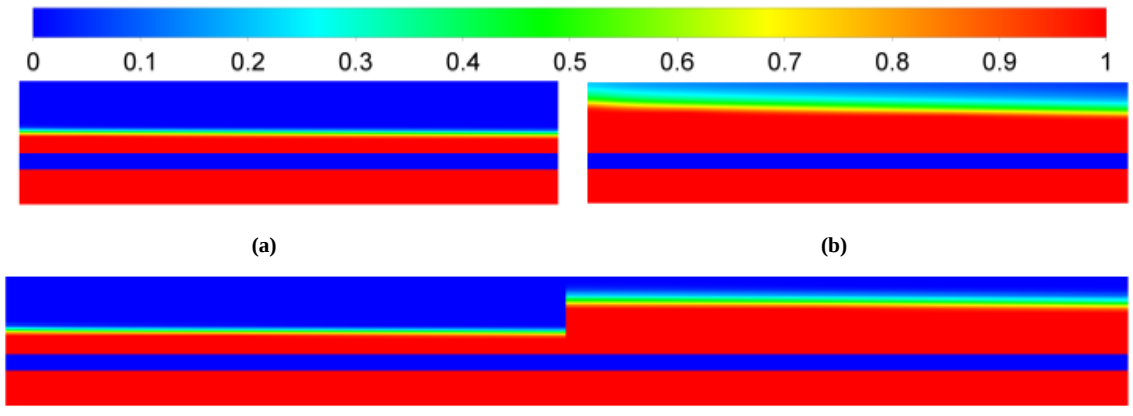

(a) **(b)**

(c)

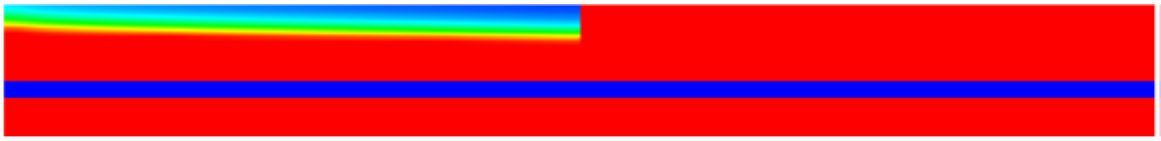

(d)

Fig. 3: Melt contours after 500 seconds; (a) Case-1, (b) Case-2, (c) Case-3 and (d) Case-4

Fig. 3 corresponds to the melt front of the PCM after 500 seconds when the inlet temperature is 300 ℃. In Fig. 3 (a, c), PCM is not incorporated with graphite, while in Fig. 3 (b, d) graphite is incorporated in PCM. The incorporation of graphite renders the anisotropic in the PCM domain; from the Fig. 3 (b, d) it is clear that the radial thermal conductivity in the composite is higher as compared to the axial direction thermal conductivity. In addition, the melt fraction is higher for the cases that contain graphite. The single PCM and cascaded LHTES unit, both shows a higher melt rate with graphite. Case-2 shows the significant rise in melt fraction as compare to case-1, and similarly, the same result can be seen between case-3 and case-4. The presence of graphite in the PCM domain significantly increases the composite's thermal conductivity, resulting in an improvement in the melting rate of PCM.

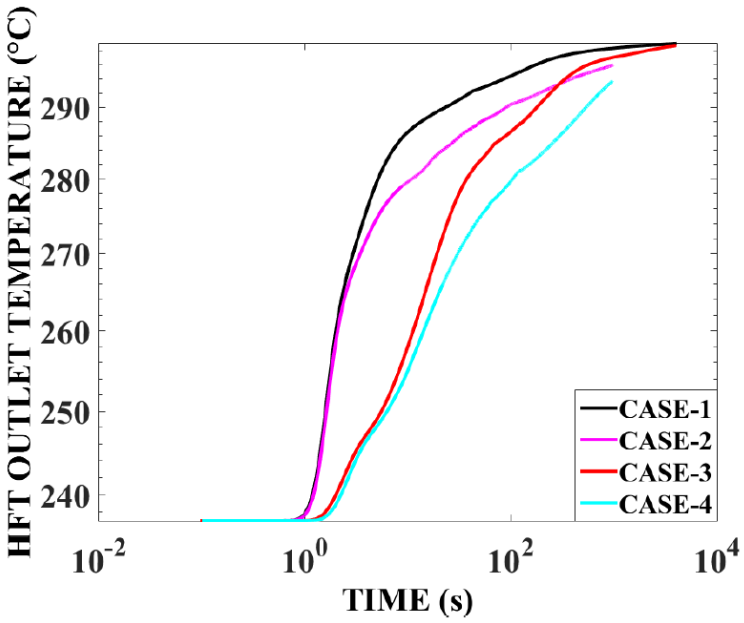

Fig. 4: HTF outlet temperature of different cases

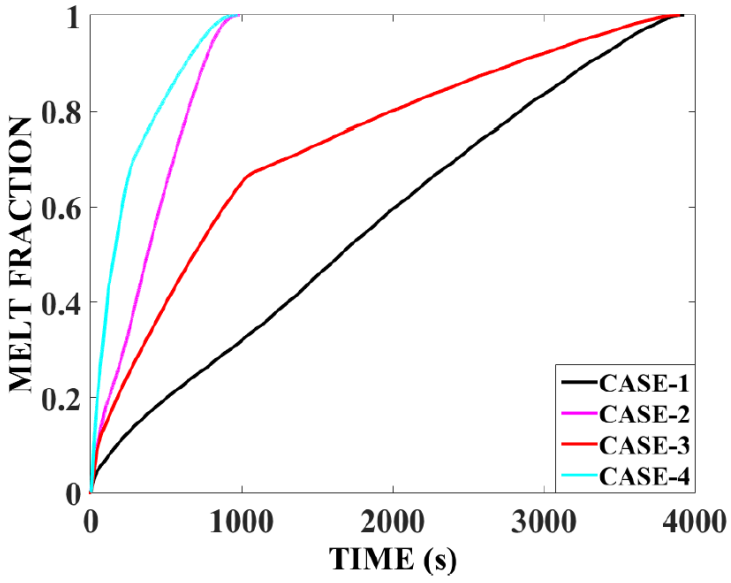

Fig. 5: Melt fraction vs Time

Fig. 4 shows the temperature profile of HTF at the outlet of the pipe with respect to time. It can be observed that the increase of the HTF temperature at the outlet is less in the case of, the enhanced thermal conductivity of the composite, the PCM with graphite. In case-2 and case-4, the HTF outlet temperature is lower as compared to case-1 and case-3, respectively. The lowering in temperature is due to the higher thermal conductivity of the composite PCM, which augment the heat transfer rate from HTF to PCM.

The melting rate of the PCM is also a parameter to measure the performance of the LHTES; a higher melting rate means an enhancement in heat transfer rate, which results in an increase in heat storage rate. Fig. 5 shows the melt-fraction profile of the PCM domain with respect to time. In case-2 and case-4, the melting of PCM is completed before case-1 and case-3, respectively, with a significant marginal of time. This shows the reduction in time to complete the charging process due to incorporation of graphite.

4.2. Effect of Cascading

Comparison between case-1 & 3 and case-2 & 4 is done to show the effect of cascading. Case- 3 and 4 correspond to the cascading of the LHTES, without graphite and with graphite, respectively.

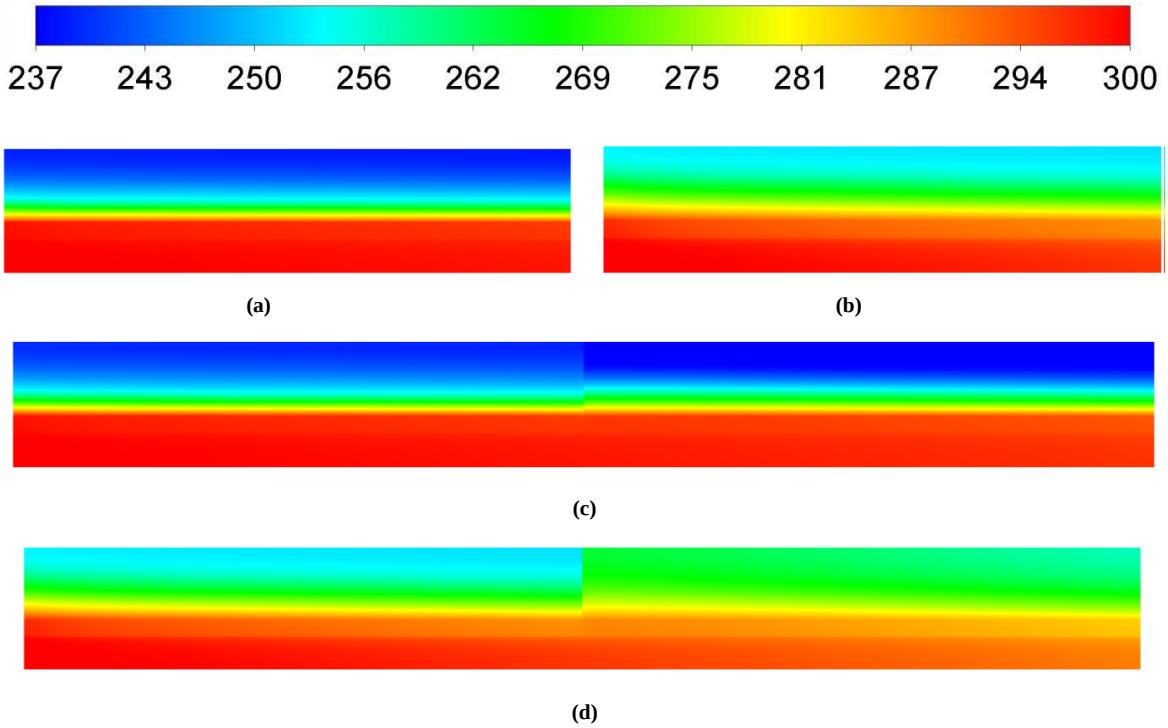

Fig. 6: Temperature contours after 500 seconds; (a) Case-1, (b) Case-2, (c) Case-3 and (d) Case-4

The incorporation of the second storage unit with a low melting temperature of PCM recovers the loss of heat through HTF. The lower melting temperature of the second PCM increases the temperature difference between the HTF and the average temperature of PCM, which results in the augmentation of the driving potential of the heat transfer. Fig. 6 shows the temperature contours of the PCM after 500 seconds when the inlet temperature is 300 ℃. Fig. 6 (c, d) represents the cascading results of the part a & b (i.e., case1 and 2), respectively. It can be observed that the temperature contours of the first storage unit of both the cases c and d are almost the same as that of the respective single PCM storage unit cases a & b. This shows the equal temperature rise in storage units, and then the second storage unit additionally accepts the heat from the HTF, which results in a temperature drop of the HTF, consequently the recovery of the heat loss.

In addition to that, in Fig. 3, the melt front of the first storage unit of the part a & c and part b & d are almost alike; this means the melting rate of first storage is the same while the addition of second storage stores the part of the remaining leaving energy. The addition of a second storage unit does not affect the total melting time, as shown in Fig. 5, because the PCM-2 (which has a lower melting temperature) completely melts before PCM-1 as shown in Fig. 7 for case-4 at 300 ℃ inlet temperature.

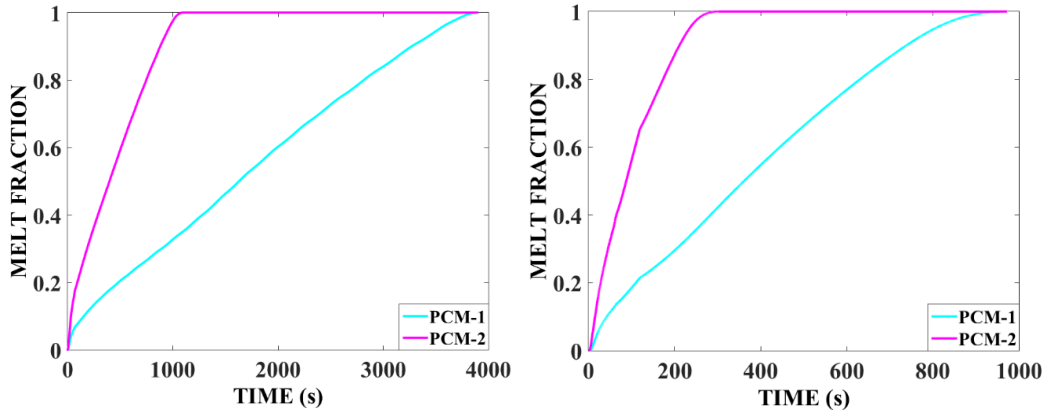

Fig. 7: Melt fraction vs time; (a) case-3 & (b) case-4

4.3. Effect of Inlet Temperature

In this section, the effect of different inlet temperatures is shown in Fig. 8. The inlet temperature of the HTF mainly increases the charging rate of the LHTES.

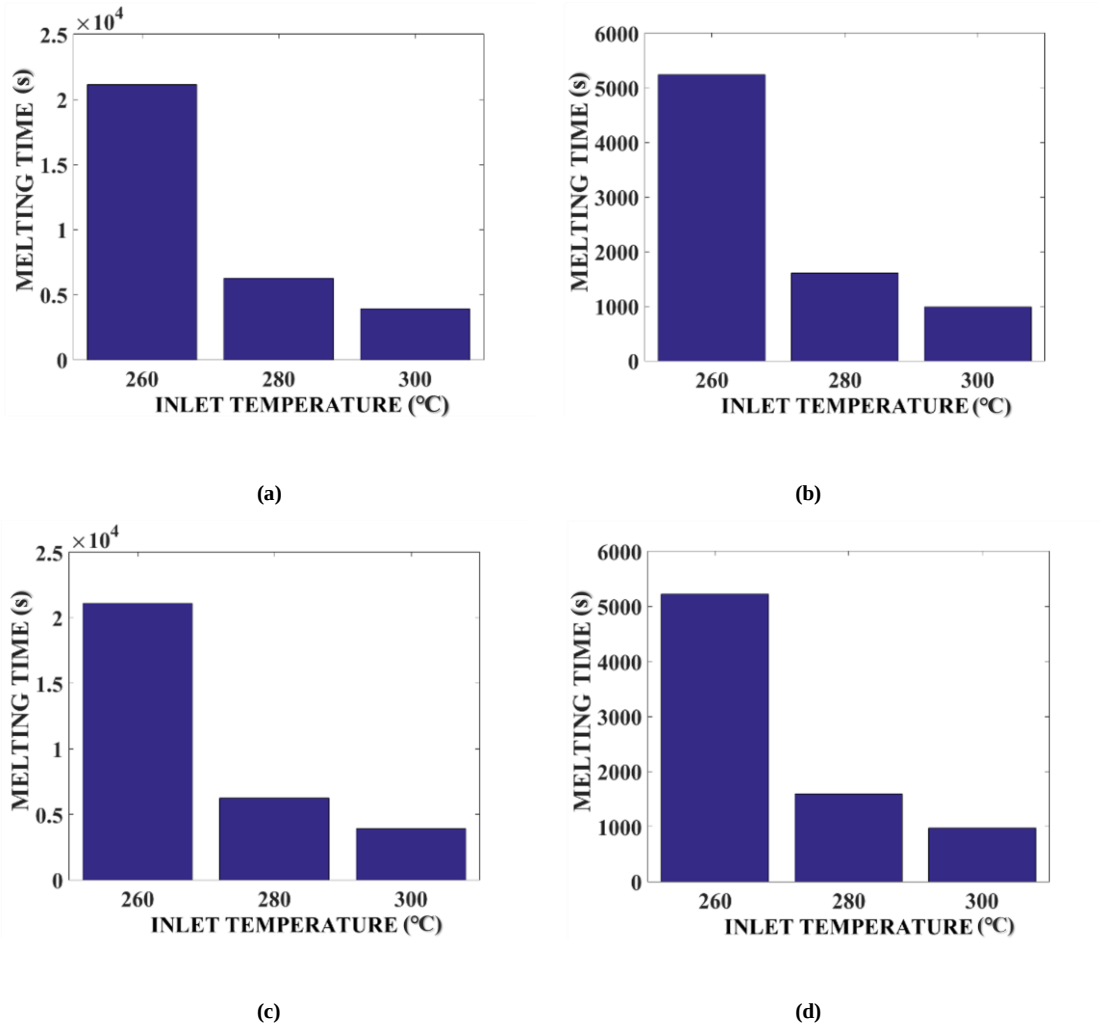

Fig. 8: Illustration of effect of intel temperature on melting time

Fig. 8 illustrates that high inlet temperature reduces the complete melting time of PCM. The HTF with high inlet temperature enters with greater amount of thermal energy and as the temperature, difference between HTF and PCM is more; the driving potential of heat transfer also more. Thus, the melting time is less in the all the cases for inlet temperature of 300 °C followed by 280 °C and 260 °C.

5. Conclusion

The numerical simulation investigates the charging dynamics of the 2-D axisymmetric shell and tube LHTES unit. In order to enhance the heat transfer rate, which reduces the melting time, graphite is incorporate in PCM, and another LHTES unit is added (cascading) to reduce the thermal energy loss. Cascading is achieved by employing two PCM's, arranged axially along the flow direction of heat transfer fluid (HTF) which is Therminol-66. PCMs selected for the energy storage are Lithium Nitrate (PCM 1) and Solar salt (PCM 2).
The analysis shows the increase in melting rate due to the enhancement of thermal conductivity of the PCM composite. The anisotropy in the thermal conductivity of composite PCM, as graphite is incorporated, renders the heat transfer in the PCM domain. The thermal conductivity in the radial direction is greater than the axial direction; therefore, the melting rate is more in the radial direction.

The cascading of LHTES reduces the energy loss at the high HTF inlet temperature. However, the cascaded LHTES unit reduces the effectiveness at lower HTF inlet temperature. The lower inlet temperature diminishes the driving potential of heat transfer due to the decrease in temperature difference between HTF and PCM; consequently, the effectiveness of the LHTES decreases.

The inlet temperature significantly affects the charging time of the LHTES. The higher inlet temperature increases the temperature difference between HTF and PCM, which increases the heat transfer potential of the system, consequently, the charging time of the LHTES reduces.

6. References

Bennon, W.D. and Incropera, F.P., 1987. A continuum model for momentum, heat and species transport in binary solid-liquid phase change systems—I. Model formulation. International Journal of Heat and Mass Transfer, 30(10), 2161-2170.

Colla, L., Fedele, L., Mancin, S., Danza, L., Manca, O., 2017. Nano-PCMs for enhanced energy storage and passive cooling applications. Applied Thermal Engineering. 110, 584-589.

Farid, M. M., Kanzawa, A., 1989. Thermal performance of a heat storage module using PCM's with different melting temperatures: mathematical modeling. Journal of Solar Energy Eng. 111, 152-7.

Farid, M. M., Kim, Y., & Kansawa, A., 1990. Thermal performance of a heat storage module using PCM's with different melting temperature: experimental. Journal of Solar Energy Eng. 112, 125-31.

Gong, Z. X., & Mujumdar, A. S., 1996. Enhancement of energy charge-discharge rates in composite slabs of different phase change materials. International Journal of Heat and Mass Transfer. 39(4), 725-733.

Gong, Z. X., & Mujumdar, A. S., 1997. Thermodynamic optimization of the thermal process in energy storage using multiple phase change materials. Applied Thermal Engineering. 17(11), 1067-1083.

Iverson, B.D., Broome, S.T., Kruizenga, A.M. & Cordaro, J.G., 2012. Thermal and mechanical properties of nitrate thermal storage salts in the solid-phase. Solar Energy, 86(10), 2897-2911.

Khan, Z., Khan, Z., & Ghafoor, A., 2016. A review of performance enhancement of PCM based latent heat storage system within the context of materials, thermal stability and compatibility. Energy conversion and management. 115, 132-158.

Kumar, R., & Verma, P. 2020. An experimental and numerical study on effect of longitudinal finned tube eccentric configuration on melting behaviour of lauric acid in a horizontal tube-in-shell storage unit. Journal of Energy Storage. 30, 101396.

Lachheb, M., Adili, A., Albouchi, F., Mzali, F. & Nasrallah, S.B., 2016. Thermal properties improvement of lithium nitrate/graphite composite phase change materials. Applied Thermal Engineering, 102, 922-931.

Li, Y. Q., He, Y. L., Wang, Z. F., Xu, C., & Wang, W., 2012. Exergy analysis of two phase change materials storage system for solar thermal power with finite-time thermodynamics. Renewable Energy. 39(1), 447-454.

Mallow, A., Abdelaziz, O., & Graham Jr, S., 2016. Thermal charging study of compressed expanded natural graphite/phase change material composites. Carbon. 109, 495-504.

Mills, A., Farid, M., Selman, J. R., & Al-Hallaj, S., 2006. Thermal conductivity enhancement of phase change materials using a graphite matrix. Applied thermal engineering. 26(14-15), 1652-1661.

Morisson, V., Rady, M., Palomo, E. & Arquis, E., 2008. Thermal energy storage systems for electricity production using solar energy direct steam generation technology. Chemical Engineering and Processing: Process Intensification, 47(3), 499-507.

Wang, J., Chen, G., & Jiang, H., 1999. Theoretical study on a novel phase change process. International journal of energy research. 23(4), 287-294.

Wu, W., Yang, X., Zhang, G., Chen, K., & Wang, S., 2017. Experimental investigation on the thermal performance of heat pipe-assisted phase change material based battery thermal management system. Energy Conversion and Management. 138, 486-492.

Xia, L., Zhang, P., & Wang, R. Z., 2010. Preparation and thermal characterization of expanded graphite/paraffin composite phase change material. Carbon, 48(9), 2538-2548.

Zhao, J., Rao, Z., Liu, C., & Li, Y., 2016. Experiment study of oscillating heat pipe and phase change materials coupled for thermal energy storage and thermal management. International Journal of Heat and Mass Transfer. 99, 252-260.

Zheng, H., Wang, C., Liu, Q., Tian, Z., & Fan, X., 2018. Thermal performance of copper foam/paraffin composite phase change material. Energy conversion and management. 157, 372-381.